ADVANCED HEALTHCARE MATERIALS
www.advhealthmat.de

In Situ Deployment of Engineered Extracellular Vesicles into the Tumor Niche via Myeloid-Derived Suppressor Cells

Silvia Duarte-Sanmiguel, Ana Panic, Daniel J. Dodd, Ana Salazar-Puerta, Jordan T. Moore, William R. Lawrence, Kylie Nairon, Carlie Francis, Natalie Zachariah, William McCoy, Rithvik Turaga, Aleksander Skardal, William E. Carson, Natalia Higuita-Castro, and Daniel Gallego-Perez**

Extracellular vesicles (EVs) have emerged as a promising carrier system for the delivery of therapeutic payloads in multiple disease models, including cancer. However, effective targeting of EVs to cancerous tissue remains a challenge. Here, it is shown that nonviral transfection of myeloid-derived suppressor cells (MDSCs) can be leveraged to drive targeted release of engineered EVs that can modulate transfer and overexpression of therapeutic anticancer genes in tumor cells and tissue. MDSCs are immature immune cells that exhibit enhanced tropism toward tumor tissue and play a role in modulating tumor progression. Current MDSC research has been mostly focused on mitigating immunosuppression in the tumor niche; however, the tumor homing abilities of these cells present untapped potential to deliver EV therapeutics directly to cancerous tissue. In vivo and ex vivo studies with murine models of breast cancer show that nonviral transfection of MDSCs does not hinder their ability to home to cancerous tissue. Moreover, transfected MDSCs can release engineered EVs and mediate antitumoral responses via paracrine signaling, including decreased invasion/metastatic activity and increased apoptosis/necrosis. Altogether, these findings indicate that MDSCs can be a powerful tool for the deployment of EV-based therapeutics to tumor tissue.

1. Introduction

Extracellular vesicles (EVs) have emerged as a promising carrier system for the delivery of therapeutic payloads for a wide variety of conditions.[1–10] EVs are cell-derived nanocarriers that mediate the transfer of bioactive cargo (e.g., nucleic acids, proteins) between cells under healthy and pathological conditions.[11–13] Compared to most nanocarrier systems for therapeutic payload delivery, EVs show improved biocompatibility, reduced immunogenicity, enhanced physicochemical stability in biofluids, and an innate ability to pass through biological barriers.[1,2,4] As such, a substantial amount of research is currently being devoted to engineering therapeutic EVs for challenging diseases like cancer. EV-based therapies, for example, have shown promise for the treatment of numerous types of cancer, including prostate cancer,[14] glioblastoma multiforme,[15] and Lewis lung carcinoma,[16,17] among others. Additional studies have also shown that EVs naturally derived from tumor cells or certain types of immune cells can drive antitumoral activity and could potentially be used as cancer vaccines.[1]

Strategies to engineer EVs generally come in two forms. The first involves loading the EVs with therapeutic cargo, which could include nucleic acids, proteins, chemotherapeutic drugs, and different types of nanomaterials, among others. The second involves functionalizing the surfaces of the EVs with different types of biomolecules to enhance targeting to specific cell/tissue types, or to reduce clearance and increase circulation time. Surface functionalization is typically done with peptides, antibodies, or aptamers. Despite the promise, however, EV-based therapeutics still face a number of challenges, including difficulties in large-scale EV manufacturing and isolation/purification, and unpredictable or poor cell/tissue targeting efficiencies.[1] Thus, new approaches are needed to facilitate targeted delivery of EV-based therapeutics to diseased tissues with more scalable manufacturing and isolation/purification procedures.

Here, we explored the use of cell therapies to achieve targeted deployment of EV-based therapies to cancerous tissue by leveraging the tumor-homing abilities of myeloid-derived suppressor

S. Duarte-Sanmiguel, A. Panic, D. J. Dodd, A. Salazar-Puerta, J. T. Moore, K. Nairon, C. Francis, N. Zachariah, W. McCoy, R. Turaga, A. Skardal, N. Higuita-Castro, D. Gallego-Perez
Department of Biomedical Engineering
The Ohio State University
Columbus, OH 43210, USA
E-mail: higuitacastro.1@osu.edu; gallegoperez.1@osu.edu

D. J. Dodd, W. R. Lawrence
Biomedical Sciences Graduate Program
The Ohio State University
Columbus, OH 43210, USA

W. E. Carson, N. Higuita-Castro, D. Gallego-Perez
Department of Surgery
The Ohio State University
Columbus, OH 43210, USA

N. Higuita-Castro
Biophysics Program
The Ohio State University
Columbus, OH 43210, USA

The ORCID identification number(s) for the author(s) of this article can be found under https://doi.org/10.1002/adhm.202101619

DOI: 10.1002/adhm.202101619

cells (MDSCs).[18,19] Tumor progression is driven by a complex interplay between different cellular compartments, including cancerous, stromal, and immune cells. Tumor-associated immune cells such as MDSCs have an innate ability to home preferentially to cancerous tissue, where they are known to exert immunosuppressive activity that favors tumor progression. This is achieved by protecting cancerous cells from the host's immune system and/or exogenous immunotherapies (e.g., CAR-T, CAR-NK cell therapies).[20–24] As such, a significant amount of research has gone into developing approaches to counteracting MDSC-driven immunosuppression in the tumor niche.[25] However, despite their innate tropism toward tumor tissue, there is currently a paucity of research on the use of MDSCs for targeted deployment of EV-based therapeutics to cancerous tissue.

To achieve targeted deployment of EV-based therapies to the tumor niche, we studied the use of MDSCs as in situ delivery vehicles of engineered EVs. MDSCs were engineered to express therapeutic cargo via nonviral electroporation of expression plasmids for *Timp3* or *Rarres2*. These two genes were chosen as model therapeutic cargo because of their role in mediating antimetastatic and antitumoral processes in cancerous tissue.[26–30] In vitro studies were conducted to evaluate the expression and loading extent and dynamics of *Timp3* and *Rarres2*, both in the transfected MDSCs and in the EVs that were released into the media. We also studied the ability of MDSC-derived EVs to transfect and modulate gene expression and function (e.g., proliferation, invasion) in cancerous cells. Finally, in vivo studies were carried out in a mouse model of breast cancer to evaluate whether engineered MDSCs still exhibited tropism toward tumor tissue, as well as potential changes in gene and protein expression and cell function in the tumor niche. MDSC-driven EV-based therapies for cancer could potentially overcome a number of limitations of current approaches to EV therapies, such as increasing their tumor-targeting abilities without the need for surface functionalization of the EVs with tumor-targeting biomolecules (e.g., simplifying manufacturing), as well as bypassing the need for inefficient EV isolation and purification procedures.

2. Results

2.1. Electroporation of Expression Plasmids for *Timp3* and *Rarres2* into MDSC Drives Transcript Overexpression and Transfer into EVs

To evaluate if MDSCs can be transfected to drive the release of engineered EVs with desirable cargo (**Figure 1**a), cultures of the murine MDSC cell line, MSC2,[18,19,31,32] were electroporated with expression plasmids for *Timp3* and *Rarres2*, and gene expression was evaluated at 12–72 h post-transfection via qRT-PCR. Sham/empty plasmids with the same backbone were used as controls. qRT-PCR analyses of the electroporated MDSCs showed significantly increased overexpression of *Timp3* and *Rarres2* for at least 12–72 h post-transfection compared to controls (Figure 1b–e). EV isolation from the supernatant and qRT-PCR analysis at 24–48 h post-transfection revealed that the EVs were markedly loaded with *Timp3* or *Rarres2* transcripts compared to EVs obtained from MDSC cultures that were electroporated with sham plasmids (Figure 1f,g). Average EV size was ≈180 nm, while EV concentrations ranged from 5×10^9–10^{10} EVs mL^{-1}. To test whether MDSC-derived EVs can be loaded with multiple different transcripts, we cotransfected *Timp3* and *Rarres2* plasmids into MDSCs and evaluated gene expression and EV loading at 24–72 h post-transfection. qRT-PCR measurements of the cells indicate that cotransfection of the two plasmids led to significantly sustained co-overexpression of *Timp3* and *Rarres2* in MDSCs for at least 72 h (Figure S1, Supporting Information). Analysis of the EVs released into the supernatant shows that the EVs were successfully coloaded with *Timp3* and *Rarres2* transcripts (Figure S1, Supporting Information), with levels comparable to those achieved with single-plasmid transfections relative to controls (Figure 1f,g). EV size and concentration ranged ≈140–160 nm, and ≈10^{10} EVs mL^{-1}, respectively. Collectively, these findings indicate that MDSCs can be readily transfected via nonviral methods, such as electroporation, and that MDSC transfection can be leveraged to drive the release of engineered EVs loaded with transcripts of the transfected cargo. Moreover, cotransfection experiments indicate that MDSC-derived EVs can also be simultaneously coloaded with different types of transcripts for therapeutic applications.

2.2. MDSC-Derived EVs are Internalized by Tumor Cells and Can Modulate Gene Expression

To evaluate if the EVs released by MDSCs following transfection can be internalized and modulate gene expression in tumor cells, we proceeded to electroporate MDSCs with *Timp3* or *Rarres2* plasmids, and isolated EVs at 24 h post-transfection, correlating with peak expression of transcripts. MDSCs electroporated with sham plasmids served as control. The isolated EVs were then dyed with a lipophilic PKH probe, and cultures of Py8119 breast cancer cells were exposed to the labeled EVs (≈10^7 EVs mL^{-1}) for 6–48 h (**Figure 2**a). Fluorescence microscopy imaging of the Py8119 cells showed successful EV uptake (Figure 2b; Figure S2, Supporting Information). qRT-PCR analyses of the Py8119 cells exposed to EVs derived from transfected MDSCs indicate that *Timp3* and *Rarres2* were significantly upregulated after 12–24 h of exposure compared to Py8119 cells exposed to control EVs derived from sham-transfected MDSCs (Figure 2c–e). No significant differences were detected after 6 h of exposure compared to controls, which is likely indicative of insufficient EV internalization and/or transcript upregulation. To verify if MDSCs mediate in situ transfer of engineered EVs and transcripts to Py8119 cells, we labeled the *Timp3*- and *Rarres2*-transfected MDSCs with a lipophilic PKH membrane dye used previously by us and others to trace EVs,[8] and proceeded to coculture MDSCs with Py8119 cells using a transwell insert. To avoid any potential confounding factors introduced by direct cell-to-cell contact, the transfected MDSCs were plated in the apical chamber, while the Py8119 cells were plated in the basal chamber (**Figure 3**a). Fluorescently labeled EVs were thus expected to be released only by the MDSCs and translocate across the 400 nm pores of the insert membrane into the Py8119 compartment. Fluorescence microscopy imaging of the basal chamber revealed that EVs released by transfected MDSCs from the apical chamber (i.e., labeled green), successfully translocated into the basal chamber, where they were internalized by the Py8119 cells (Figure 3b; Figure S3, Supporting Information). qRT-PCR analysis of the Py8119 cells showed clear

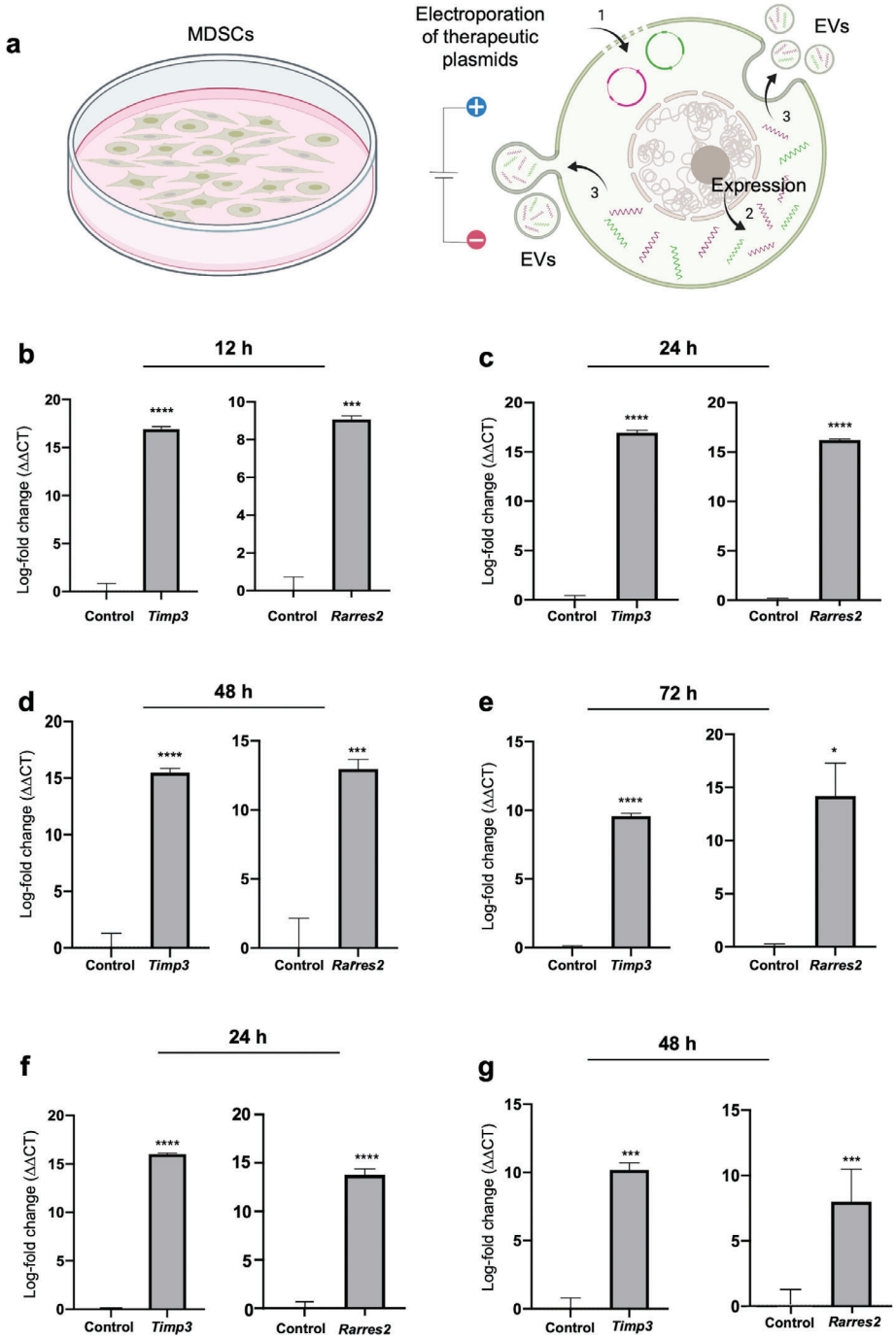

Figure 1. Nonviral transfection of MDSCs mediates the release of engineered EVs with desirable cargo. a) Schematic diagram illustrating the experimental design. 1) MDSCs were electroporated with expression plasmids for *Timp3* or *Rarres2*. Electroporation with sham/empty plasmids served as control. 2) The plasmids are expressed within the MDSCs and 3) transcripts are packed and released within EVs. qRT-PCR analysis of the MDSC cultures at b) 12, c) 24, d) 48, and e) 72 h post-electroporation reveals strong *Timp3* or *Rarres2* overexpression. Analysis of the EVs isolated from the supernatant at f) 24 and g) 48 h post-electroporation indicates successful loading of the EVs with *Timp3* or *Rarres2*. * $p < 0.05$ ($n = 4$), *** $p < 0.01$ ($n = 3$), **** $p < 0.0001$ ($n = 4$).

overexpression of *Timp3* and *Rarres2* compared to Py8119 cells that were cocultured with MDSCs transfected with sham plasmids (Figure 3c). Moreover, dead cell staining with propidium iodine in the Py8119 compartment suggests a cytotoxic effect of *Timp3*- and *Rarres2*-loaded EVs, which was absent for sham-loaded EVs. Altogether, these findings indicate that EVs released by transfected MDSCs have the ability to mediate in situ gene transfer and overexpression of therapeutic cargo in cancer cells in a paracrine manner, which could potentially be leveraged for the deployment of EV-based therapies in the tumor niche.

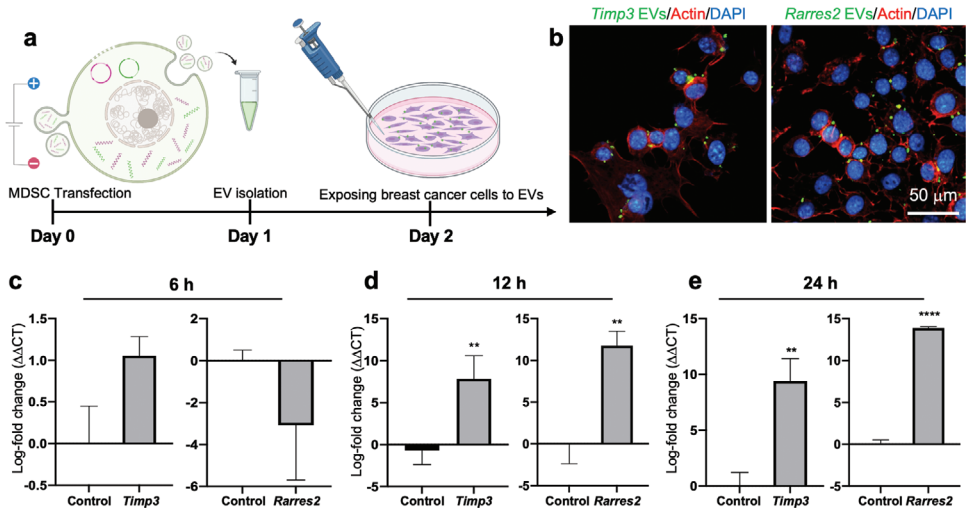

Figure 2. MDSC-derived EVs can be internalized by cancer cells and modulate gene expression. a) Schematic diagram illustrating the experimental design. MDSCs were electroporated with expression plasmids for *Timp3* or *Rarres2*. Electroporation with sham/empty plasmids served as control. MDSC-derived EVs were isolated and incubated with Py8119 mouse breast cancer cell cultures for 6–24 h. b) Fluorescence microscopy imaging of the Py8119 cells (labeled red and blue) revealed successful uptake of MDSC-derived EVs (labeled green). The images shown represent EV uptake at 24 h post-exposure. qRT-PCR analysis of the Py8119 cultures at c) 6, d) 12, and d) 24 h post-EV exposure reveals strong *Timp3* or *Rarres2* overexpression after 12 h of exposure. ** $p < 0.01$ ($n = 4$), **** $p < 0.0001$ ($n = 4$).

2.3. Transfected MDSCs Hinder Tumor Cell Proliferation and Invasion Capabilities In Situ

Once we established a paracrine role for MDSC-derived engineered EVs in the modulation of cancer cell responses (e.g., gene expression and viability, Figure 3), we proceeded to evaluate if MDSCs transfected with *Timp3* and *Rarres2* plasmids could influence tumor cell proliferation and invasion, in situ. For this, *Timp3*- or *Rarres2*-transfected MDSCs and Py8119 cells were mixed and cocultured in direct contact at a 1:1 ratio to emulate more closely the degree of cell-cell interactions within the tumor niche (**Figure 4**a).[19,33–35] Cocultures with MDSCs transfected with sham plasmids served as control. The cells were pre-labeled with different fluorescent dyes to be able to distinguish them during the analysis phase (i.e., Green: transfected MDSCs; Red: Py8119 breast cancer cells). For proliferation assays, Py8119 cell numbers were quantified by flow cytometry after 24 h of coculture. For invasion assays, the cells were plated on Matrigel-coated transwell inserts (Corning BioCoat Matrigel Invasion chambers), and the number of Py8119 cells that invaded through the insert over a period of 24 h was visualized and quantified with fluorescence microscopy (Figure 4b). Flow cytometry analyses revealed a significant decrease in the number of Py8119 cells when cocultured with *Timp3*- or *Rarres2*-transfected MDSCs compared to cocultures with sham-transfected MDSCs, with a more pronounced oncolytic effect seen for *Rarres2* compared to *Timp3* (Figure 4c). Decreased cancer cell numbers could be potentially driven by EV-mediated cell death, as shown in Figure 3c. Moreover, invasion assays revealed that Py8119 cells cocultured with *Timp3*- or *Rarres2*-transfected MDSCs had a tendency to show decreased invasion activity compared to controls (Figure 4d). Overall, these findings indicate that transfected MDSCs have the ability to modulate key cancer cell behaviors such as proliferation and invasion, in situ, possibly via the release of engineered EVs loaded with transcripts of the therapeutic cargo, as suggested by the results in Figure 3.

2.4. Transfected MDSCs Retain Tumor-Homing Capabilities and Modulate Gene and Protein Expression in the Tumor Niche In Vivo

To evaluate whether electroporation with expression plasmids for therapeutic cargo impacted the tropism of MDSCs toward tumor tissue, we proceeded to inject *Timp3*- and *Rarres2*-transfected MDSCs into the tail vein of tumor-bearing mice (**Figure 5**a). In vivo tumor homing of MDSCs was evaluated via IVIS imaging. For these experiments, we used an orthotopic xenograft model of nude/immunocompromised mice injected with human breast cancer cells (MDA-MB-231 cells) in the mammary gland. The tumors were allowed to reach a size of approximately 5 mm before the transfected MDSCs were injected. Immediately prior to injection, transfected MDSCs were fluorescently labeled with a cell tracker membrane dye to detect the location of the cells and trace the EVs released within the tumor niche. After 24 h, the mice were sacrificed and IVIS imaging was used to evaluate the accumulation of fluorescence signal stemming from the cell tracker probe in the tumor. IVIS results indicated a strong accumulation of transfected MDSCs in the tumor niche compared to other organs (Figure 5b), suggesting that episomal expression of the therapeutic plasmid cargo did not significantly impact the ability of MDSCs to home to cancerous tissue. Ex vivo studies with microfluidic systems incorporating two different types of breast tumor organoids (i.e., aggressive/mesenchymal Py8119 and epithelial Py230),[19] and nontumoral cells (i.e., primary mouse embryonic fibroblasts or pMEFs), further showed that MDSCs transfected with therapeutic or sham cargo/plasmids appear to show similar levels of invasiveness and accumulation in the

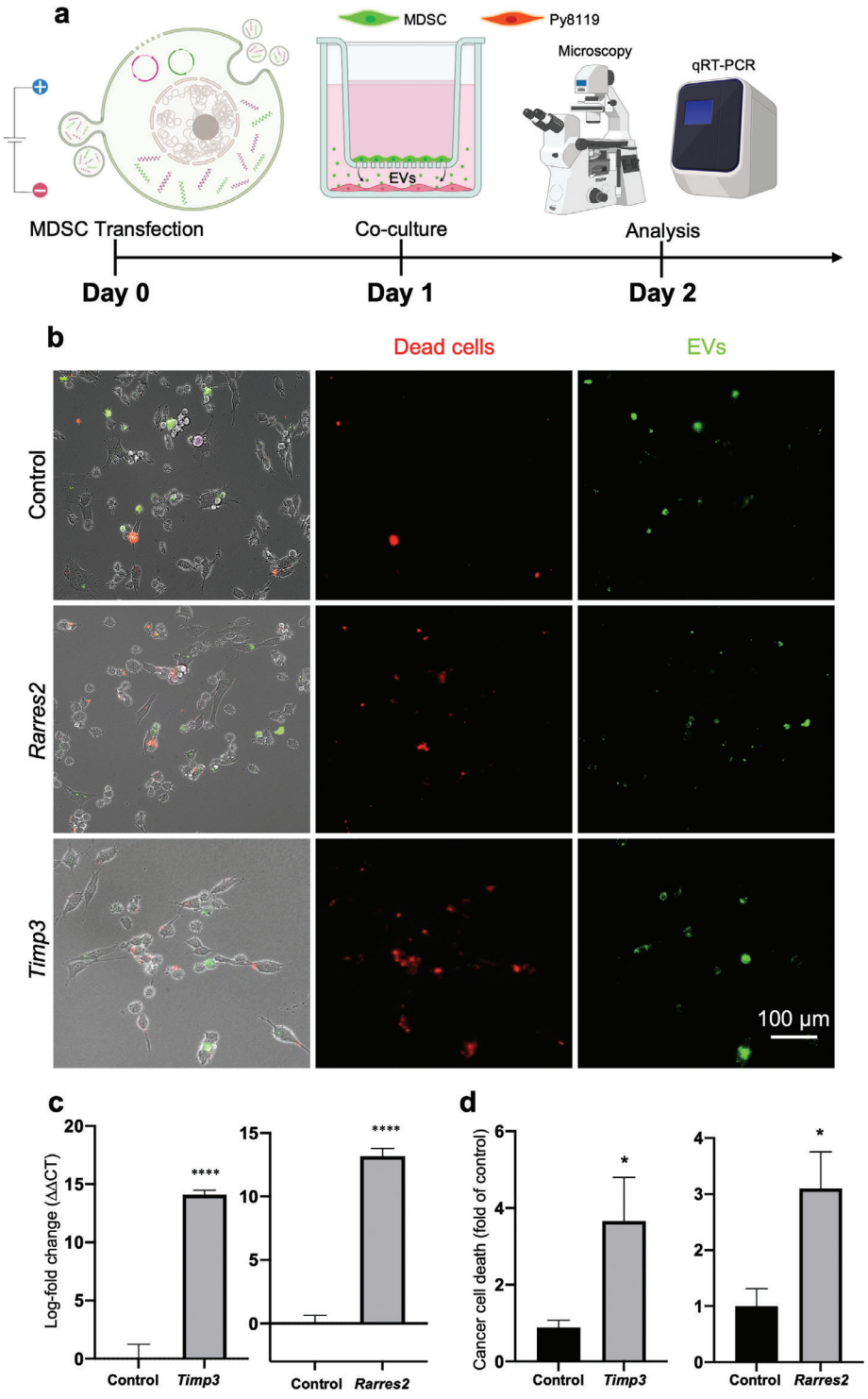

Figure 3. Transfected MDSCs can transfer engineered EVs to breast cancer cells, in situ, and mediate gene expression and cellular responses. a) Schematic diagram illustrating the experimental design. MDSCs were electroporated with expression plasmids for *Timp3* or *Rarres2*. Electroporation with sham/empty plasmids served as control. Transfected MDSCs and Py8119 mouse breast cancer cells were cocultured using a transwell system, with the MDSCs in the apical chamber and Py8119 cells in the basal chamber. The MDSCs were-prelabeled with a membrane dye to trace EV release and uptake. MDSC-derived EVs were thus expected to translocate across the membrane and interact with Py8119 cells in the basal chamber. b) Fluorescence microscopy imaging of the Py8119 cultures revealed successful translocation and uptake of MDSC-derived EVs (green). Py8119 cells with compromised cell viability/membrane integrity were labeled red. c) qRT-PCR analyses of the Py8119 cultures showed marked overexpression of *Timp3* or *Rarres2* after 24 h. d) Viability analyses suggest an oncolytic effect for MDC-derived EVs loaded with *Timp3* or *Rarres*2 compared to sham MDSC-derived EVs. * $p < 0.05$ ($n = 10$), **** $p < 0.0001$ ($n = 4$).

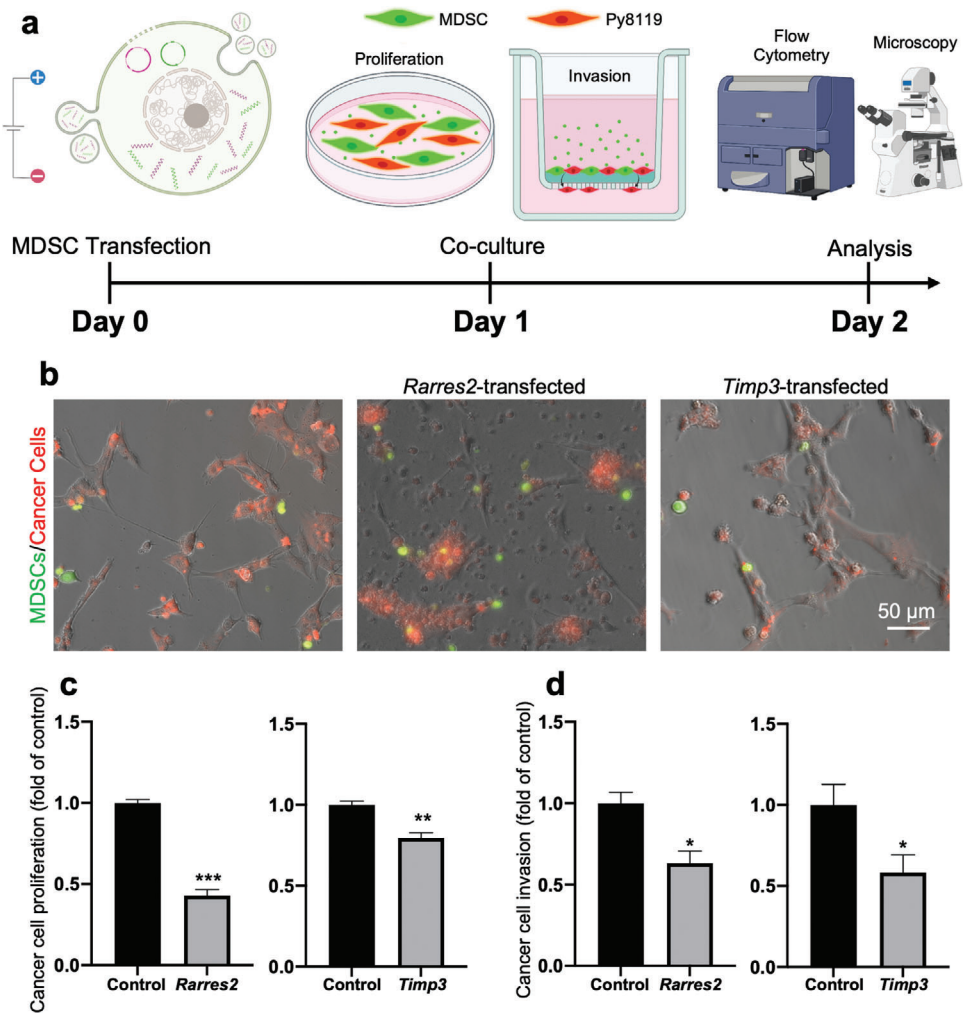

Figure 4. Transfected MDSCs can also modulate cancer cell proliferation and invasion, in situ. a) Schematic diagram illustrating the experimental design. MDSCs were electroporated with expression plasmids for *Timp3* or *Rarres2*. Electroporation with sham/empty plasmids served as control. Transfected MDSCs and Py8119 mouse breast cancer cells were cocultured in direct contact. Matrigel-coated transwell insets were used for cell invasion studies. The MDSCs were-prelabeled green, and the Py8119 cells were prelabeled red. b) Fluorescence microscopy imaging of the MDSC/Py8119 cocultures after 24 h. c) Flow cytometry analysis revealed reduced Py8119 cell numbers in cocultured with *Timp3*- or *Rarres2*-transfected MDSCs. d) Py8119 cell invasion analyses showed reduced Py8119 cell invasion capabilities in cocultures containing *Timp3*- or *Rarres2*-transfected MDSCs. * $p < 0.05$ ($n = 4$), ** $p < 0.01$ ($n = 4$), *** $p < 0.005$ ($n = 3$).

different organoids (Figure S4, Supporting Information). Additional in vivo studies suggest little to no accumulation of MDSCs in clearance organs such as the liver (Figure S5, Supporting Information). qRT-PCR analysis and immunostaining of the collected tumor tissue confirmed localized overexpression of *Timp3* and *Rarres2* at the mRNA and protein levels compared to controls (Figure 5d–g). Fluorescence imaging of the cell membrane tracker dye, which in addition to helping localize the injected MDSCs, can also be used to trace MDSC-derived EVs, appears to show MDSC-derived EV uptake by other cells within the tumor niche (Figure S6, Supporting Information). Moreover, additional immunostaining revealed a decrease in proliferation activity based on reduced Ki67 immunoreactivity, as well as an increase in pro-apoptotic activity based on enhanced cleaved Caspase-3 immunoreactivity in the tumor niche compared to mice injected with control MDSCs (Figure S7, Supporting Information). Altogether, these findings suggest that transfected MDSCs still show remarkable tropism toward tumor tissue, where they can mediate the deployment and transfer of therapeutic EVs into tumor-resident cells and drive overexpression of therapeutic cargo, abrogating pro-tumoral activity.

3. Discussion

This study reports on a novel approach to deploying EV-based therapeutics into the tumor niche in a targeted manner via the use of MDSC-driven cell therapies. EVs have been shown to offer a number of advantages for therapeutic payload delivery for cancer compared to many other micro- or nano-carrier systems.[36–38] However, targeted delivery of EVs to cancerous tissue requires complex surface engineering processes that often yield inefficient and/or unpredictable targeting outcomes. Additional

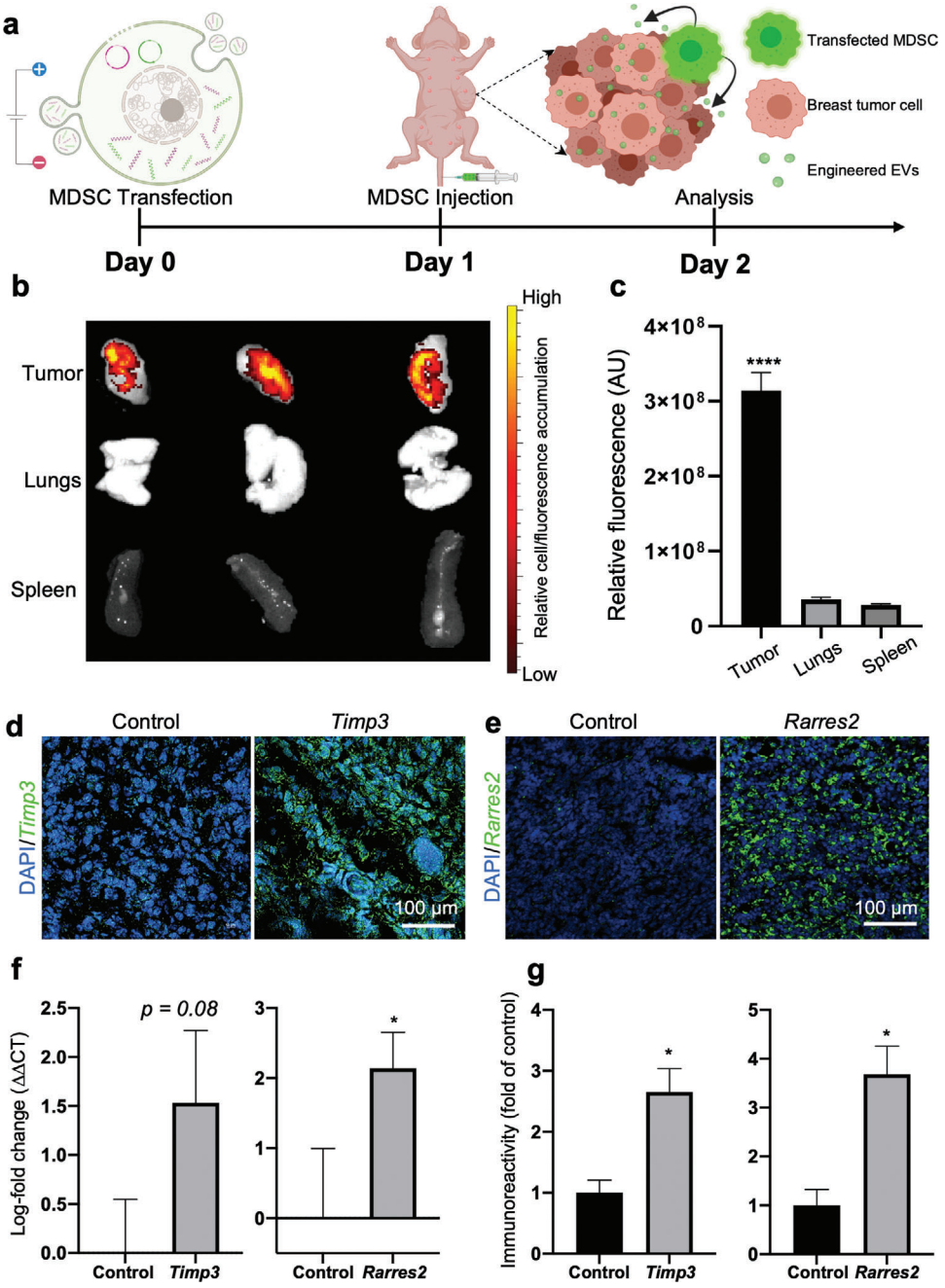

Figure 5. Transfected MDSCs retain tumor-homing abilities and drive antitumoral gene and protein expression. a) Schematic diagram illustrating the experimental design. MDSCs were electroporated with expression plasmids for *Timp3* or *Rarres2*. Electroporation with sham/empty plasmids served as control. Transfected MDSCs were then injected into tumor-bearing mice via the tail vein, and accumulation and gene/protein expression in the tumor was evaluated after 24 h. b,c) IVIS imaging after 24 h revealed strong accumulation of transfected MDSCs in the tumor niche compared to other organs. Transfected MDSCs were fluorescently pre-labeled red for these experiments. d–g) Tumor tissue analyses indicate marked expression of the therapeutic cargo, *Timp3* or *Rarres2*, both at the d,e,g) protein and f) transcript levels. * $p < 0.05$ ($n = 5$), **** $p < 0.0001$ ($n = 6$).

challenges to EV-based therapeutics for cancer include difficulties in identifying scalable and efficient EV biomanufacturing and isolation/purification procedures. Thus, there is still a need for novel platform technologies that enable targeted deployment of EV-based therapies to cancerous tissue. MDSCs are immature innate immune cells that are highly expanded in cancer patients,[20] and are known to exhibit a high degree of tropism toward tumor tissue, where they contribute to the loss of immune effector cell function. We have previously shown in ex vivo and in vivo studies that MDSCs exhibit high dissemination and tumortropic capabilities at the single-cell level, as well as contact-guided motility similar to tumor cells.[18,19,39–42] Thus, pharmacologically

counteracting the infiltration of MDSCs into the tumor niche and halting their immunosuppressive activity has emerged as an attractive therapeutic strategy against cancer. However, efforts to effectively stem or reverse MDSC-driven immunosuppression in tumor tissue have been hampered by the lack of druggable targets.[43] Nevertheless, MDSC homing to tumor tissue could potentially be leveraged to deploy therapies to cancerous tissue in a more targeted manner. While myeloid cells have been recently studied as therapeutic carriers in cancer,[44,45] to the best of our knowledge, no study has investigated the use of MDSCs to drive engineered EV-based therapies in cancerous tissue to date.

While our results indicate that MDSC-based deployment of therapeutic EVs in breast cancer may be feasible, it is important to point out that, compared to direct delivery of EVs, using cell therapies as an EV delivery vehicle could potentially limit deployment to certain locations protected by biological barriers that are otherwise easily overcome by EVs (e.g., blood brain barrier).[46,47] Although this is clearly an important issue meriting further study, there is evidence that MDSCs can traffic to brain tissue in certain malignancies or in other neurodegenerative conditions.[48–54] Thus, the use of MDSCs as a platform technology for EV deployment may still be feasible for some applications where biological barriers are present.

Additional challenges potentially stemming from the use of cells to deploy EV therapies could include limited cell availability. However, accumulating evidence suggests that the circulating levels of MDSCs tend to be significantly elevated in cancer patients, and under other non-neoplastic conditions (e.g., stroke, Alzheimer's disease).[33,50,55–57] Thus, isolating and expanding MDSCs from circulation for subsequent use as a therapeutic agent, similar to the methods used for CAR-T or CAR-NK cell therapies, is likely a feasible strategy for the implementation of MDSC-driven EV therapies under multiple conditions (besides cancer). Moreover, additional studies have shown that peripheral blood mononuclear cells (PBMCs) can be differentiated toward MDSCs or MDSC-like cells[32,58] in vitro, making PBMCs another potential source of MDSCs for therapeutic applications.

In this study, MDSC-derived EVs were engineered to contain transcripts of *Timp3* or *Rarress2*. The *Rarres2* gene encodes for a small protein that is functionally downregulated in various cancers, including adrenocortical carcinomas, melanoma, and breast cancer,[59] which contributes to dysregulation of the Wnt/β-catenin signaling pathway and tumor progression.[29,60] The *Timp3* gene, on the other hand, falls into the family of tissue inhibitors of metalloproteinases. *Timp3* is a well-known inhibitor of cancer cell function, especially invasion, in numerous cancer types, including breast cancer.[28,61,62] Our results clearly indicate that MDSC-based deployment of *Timp3*- or *Rarres2*-loaded EVs results in decreased viability and invasion capabilities in breast cancer cell cultures, as well as reduced proliferation and increased pro-apoptotic activity in vivo. MDSC-derived EVs, however, could conceivably be engineered to contain a wide variety of therapeutic cargo/transcripts besides *Timp3* or *Rarres2*. For example, immunomodulatory transcripts such as *IL-12* could potentially be loaded into MDSC-derived EVs to drive more effective immune responses against tumors.[45] Moreover, in addition to cancer, MDSCs are also known to infiltrate diseased tissue in other conditions, including stroke and Alzheimer's disease. Therefore, the use of engineered MDSCs as EV delivery vehicles could conceivably go beyond cancer applications, and as such, different genes/transcripts would have to be explored depending on the therapeutic target.

Importantly, our results indicate that, despite potential phenotypic changes following transfection, engineered MDSCs maintain preferential tropism toward the tumor microenvironment, with little-to-no accumulation in off-target tissues such as the liver, which provides crucial evidence for the viability of this immunotherapy. MDSC migration to the tumor microenvironment is mediated by an array of cytokines and chemokines, primarily CCL2, but also other CXC-motif chemokines.[63] While our data suggest that these recruitment mechanisms are likely maintained in engineered MDSCs, it is possible that the degree of engineered MDSC tropism toward diseased tissue versus off-target accumulation could be impacted by the method used to transfect the MDSCs (e.g., nonviral versus viral approaches),[64–72] and/or the type of cargo/transcript that is overexpressed in them. Thus, future studies should continue to evaluate how these parameters influence MDSC and MDSC-derived EV targeting to diseased tissues, as well as the potential consequences of off-target secretion of the EVs and corresponding therapeutic payloads in other tissues.

4. Conclusions

Our results indicate that a single nonviral transfection of MDSCs with expression plasmids for therapeutic cargo is sufficient to drive the production of engineered EVs loaded with transcripts of the transfected cargo. MDSC-derived EVs were shown to be effectively internalized by tumor cells and to modulate gene expression and tumor cell responses. Notably, when deployed systemically in circulation, transfected MDSCs still exhibited a remarkable ability to home to tumor tissue, where they were shown to mediate engineered EV transfer into the tumor niche and promote overexpression of therapeutic cargo. Using MDSCs to deliver therapeutic EVs to cancerous tissue has the potential to overcome some of the major limitations of current approaches to EV-based therapeutics for cancerous tissue, including bypassing the need for complex EV isolation and purification procedures, as well as the need for surface functionalization with cancer-targeting biomolecules, thus simplifying the manufacturing process. Altogether, our findings indicate that nonvirally transfected MDSCs could potentially serve as a powerful platform technology for the deployment of EV-based therapeutics to cancerous tissue.

5. Experimental Section

Cell Culture: The mouse mammary cancer cell lines used in this study were derived from MMTV-PyMT transgene-induced mammary tumors in C57BL/6 mice (ATCC, Manassas, VA). The two cell lines used, Py8119 and Py230, were derived from the same tumor model but have distinct mesenchymal (Py8119) or epithelial-like (Py230) features.[42] The cells were kept in culture with F-12/Kaighn's medium supplemented with 5% fetal bovine serum (FBS) and 0.1% MITO+ Serum Extender (Corning). The murine MDSC cell line, MSC2 (gift from Gregoire Mignot to Dr. William E. Carson), was cultured in RPMI medium (Gibco, Dublin,IE) containing 10% FBS, 1% sodium pyruvate (Gibco) and 1% antibiotic-antimycotic (Gibco). All the cells were maintained at 37 °C, 5% CO_2 and 95% humidity.

Electroporation of MDSCs: MSC2 cells were transfected via bulk electroporation with either sham or treatment (*Timp3*, *Rarres2*) expression

Table 1. List of DNA plasmids used in this study.

Plasmid vector	Company	Cat. No	Backbone
Sham	Origene	PS100001	pCMV6
Timp3 (Mouse tissue inhibitor metalloproteinase 3)	Origene	MG202295	pCMV6
Rarres2 (Mouse retinoic acid receptor responder)	Origene	MG222586	pCMV6

plasmids using a Neon Transfection System (ThermoFisher). Transfected MDSCs were cultured in RPMI medium (Gibco, Dublin, IE) containing 10% exosome-depleted FBS and 1% sodium pyruvate. A full list of plasmids used in this study can be found in **Table 1**.

EV Isolation and Characterization: The culture media of transfected MDSCs was collected and centrifuged at 2000 × *g* for 20 min at 4 °C to pellet down and remove dead cells and debris. The supernatant was mixed with Total Exosome Isolation Reagent (Invitrogen, 44-783-59) at a 1:2 ratio and incubated at 4 °C overnight. The solution was then centrifuged at 10000 RPM for 60 min at 4 °C to precipitate the EVs. To quantify EV size and concentration, EV pellets were re-suspended in 1 mL of serum-free media and analyzed using a Nanosight NS300.

Exposure of Breast Cancer Cell Cultures to EVs: To evaluate the uptake and transfer of transcripts from MDSC-derived EVs to cancer cells, Py8119 cells were exposed to MDSC-derived EVs loaded with *Timp3* or *Rarres2*. EVs were collected and quantified 24 h post-transfection, as described previously. Py8119 cells were seeded on laminin-coated cover slips (Neuvitro, GG-12-15-Laminin) at a density of 1.5×10^5 cells per replicate and cultured in Ham's F-12K (Kaighn's) medium supplemented with 5% EV-free FBS and 1% antibiotic-antimycotic 12h prior to EV exposure. To visualize EV uptake by recipient Py8119 cancer cells, isolated EVs were stained using a PKH67 Green Fluorescent Cell Linker membrane dye kit (Millipore Sigma, MINI67-1KT). Each Py8119 cell replicate was exposed to $\approx 10^7$ EVs. Three independent experiments were run with exposures lasting 6, 12, and 24 h. Following EVs exposure, the cells were fixed with 10% formalin solution. Phalloidin-iFluor 555 (Abcam, ab176756) was used to stain actin filaments and help visualize Py8119 cells better. The cells were imaged using a Nikon TI2-E fluorescence microscope operating on NIS-Elements AR v5.20.

In Situ Tracing of EV Release and Capture: To evaluate the transfer of EVs from MDSCs to cancer cells, transfected MDSCs and Py8119 cells were cocultured in 6-well transwell plates (Corning, 3450). MDSCs were stained with a PKH67 green fluorescence dye following transfection, and plated in the apical chamber at a density of 2.5×10^5 cells per well. Py8119 cells were seeded in the basal chamber at the same density. The cocultures were incubated for 24 h at 37 °C, 5% CO_2, and 95% humidity. Following this, Py8119 cell viability was evaluated using ethidium homodimer (Invitrogen, L3224). The Py8119 cells were then imaged using a Nikon TI2-E fluorescence microscope operating on NIS-Elements AR v5.20. MDSC-derived EVs were imaged under the green fluorescence channel, and Py8119 cells with compromised viability/membrane integrity were imaged under the red fluorescence channel.

Cancer Cell Proliferation Assays: Cell proliferation studies were performed using cocultures of transfected MDSCs and Py8119 cells. Py8119 cells were stained with CellTracker red (Invitrogen, 34 552) and seeded at a density of 1.5×10^5 per well in 6-well plates. Transfected MDSCs were stained with CellTracker green (Invitrogen, C7025) and coplated with the cancer cells at a 1:1 ratio. The cocultures were incubated at 37 °C, 5% CO_2, and 95% humidity for 24 h, and imaged with a Nikon TI2-E fluorescence microscope operating on NIS-Elements AR v5.20. Py8119 cell (red) numbers were quantified via flow cytometry using an LSRII flow cytometer (BD Biosciences).

Cancer Cell Invasion Assays: Cell invasion studies were performed using the BioCoat Matrigel Invasion Chamber (Corning, 354 480) according to the manufacturer's protocol. Py8119 cells were stained with CellTracker and then coseeded with transfected MDSCs (1:1 ratio) in each insert. The plates were then incubated for 24 h at 37 °C to allow for cancer cell invasion. Invasion was directed across the inserts by establishing an EV-free FBS gradient. Cancer cells that invaded across the membrane were imaged using a Nikon TI2-E fluorescence microscope and quantified using Image J software (National Institutes of Health, Bethesda, MD).

Orthotopic Tumor Xenografts: Immunodeficient nude mice (Jackson Laboratory), 6–8-week-old, were injected with 10^6 human breast cancer cells MDA-MB-231 (ATCC) suspended in 100 µL of 7 mg mL^{-1} basement membrane matrix (Trevigen) in the lower right abdominal mammary fat pad to generate tumors. In some instances, to trace the release and uptake of MDSC-derived EVs, the breast cancer cells were fluorescently prelabeled with a green MemGlow dye (Cytoskeleton).

In Vivo Tumor Homing Studies: Transfected MDSCs were stained using PKH67 red membrane dye (Millipore Sigma) prior to injection. Tumor-bearing mice were then injected with $\approx 10^6$ MDSCs via the lateral tail vein. Mice were sacrificed 1-day post-injection, and the tumors, lungs and spleens were characterized with an IVIS Imaging System (Xenogen Imaging Technologies). All animal studies were performed in accordance with protocols approved by the Laboratory Animal Care and Use Committee of The Ohio State University (2016A00000074-R1).

Immunostaining: All the antibodies used in this study are listed in **Table 2**. OCT-embedded tumors were sectioned at 10 µm and mounted in charged microscopy slides. Tissue sections were fixed in cold methanol, blocked with 10% normal goat serum or mouse on mouse (M.O.M.) blocking reagent, and incubated with specific primary antibodies and subsequently with fluorescently tagged secondary antibodies. Tissue sections were imaged using a Nikon TI2-E fluorescence microscope operating on NIS-Elements AR v5.20.

Table 2. List of antibodies used in this study.

Target	Primary Antibody	Raised	Cat. No.	Company	Conc.	Secondary antibody	Conc.
Timp3	Timp3	Rabbit	ab39184	Abcam	1:250	Goat pAb to rabbit IgG 488 (H+L)	1:200
Chemerin	Rarres2	Rabbit	ab103153	Abcam	1:500	Goat pAb to rabbit IgG 488 (H+L)	1:200
Ki67	Ki67	Rabbit	ab15580	Abcam	1:200	Goat pAb to rabbit IgG 488 (H+L)	1:200
Cleaved Capsase-3	Caspase-3 (mouse)	Rabbit	ab449	Abcam	1:50	Goat pAb to rabbit IgG 647 (H+L)	1:200

Table 3. List of primers used for gene expression analysis.

Gene Symbol	Gene name	Gene aliases	Species	Company	Cat. No.
Gapdh	glyceraldehyde-3-phosphate dehydrogenase	Gapdh	Mouse	Thermofisher Scientific	Mm99999915_g1
Timp3	Metallopeptidase inhibitor	TIMP-3	Mouse	Thermofisher Scientific	Mm033403204_m1
Rarres2	Retinoic acid receptor	AI303516	Mouse	Thermofisher Scientific	Mm00503579_m1
ATP6	ATP synthase F0 subunit 6	Gm10925	Mouse	ThermoFisher Scientific	Mm03649417_g1

Gene Expression Analyses: Total RNA was extracted using TRIzol reagent (ThermoFisher). Reverse transcription reactions were performed using 500–1000 ng RNA in a 20 µl reaction with the superscript VILO cDNA synthesis kit (ThermoFisher). cDNA was used as a template to measure expression levels by quantitative real-time PCR using predesigned primers. Real-time PCR reactions were performed using the QuantStudio 3 Real-Time PCR System with TaqMan fast advance chemistry (Thermo Scientific) with the following conditions: 95 °C 10 min, 40 cycles of 95 °C 1 min, 60 °C 1 min, and 72 °C 1 min. Gene expression was normalized against the house keeping genes *GAPDH* and *ATP-6*. A full description of primers can be found in **Table 3**.

Statistical Analysis: All data are reported as the mean and standard error. Statistical analyses were completed using SigmaPlot v14.0 and Prism v10. Comparisons between groups were performed based on 3–10 biological replicates. Statistical outliers (i.e., >3 studentized standard deviations) were excluded from the analyses.

Supporting Information

Supporting Information is available from the Wiley Online Library or from the author.

Acknowledgements

Funding for this work was partly provided by a New Innovator Award (NIBIB/NIH, Grant No. DP2EB028110) and Grant No. DP1DK126199 to D.G.-P. Most illustrations were created using BioRender.com.

Conflict of Interest

The authors declare no conflict of interest.

Author Contributions

S.D.-S., A.P., and D.D. contributed equally to this work. The idea was conceived by D.G.-P. and N.H.-C. D.G.-P. and S.D.-S. oversaw experimental design. In vitro and in vivo experiments were run by S.D.-S., A.P., D.D., A.S.-P., J.T.M., W.R.L., C.F., N.Z., B.M., and R.T. Ex vivo organoid experiments were conducted by K.N. under the supervision of A.S. W.E.C. provided expertise and guidance in MDSC and cancer biology. The manuscript was written by D.G.-P. with the support of S.D.-S., A.P., D.D., and N.H.-C. All coauthors provided feedback on the manuscript.

Data Availability Statement

The data that support the findings of this study are available from the corresponding author upon reasonable request.

Keywords

extracellular vesicles, myeloid-derived suppressor cells, nonviral gene and cell therapies, solid tumors, tumor tropism

Received: August 6, 2021
Revised: September 26, 2021
Published online: October 27, 2021

[1] X. Zhang, H. Zhang, J. Gu, J. Zhang, H. Shi, H. Qian, D. Wang, W. Xu, J. Pan, H. A. Santos, *Adv. Mater.* **2021**, *33*, 2005709.
[2] O. M. Elsharkasy, J. Z. Nordin, D. W. Hagey, O. G. de Jong, R. M. Schiffelers, S. E. Andaloussi, P. Vader, *Adv. Drug Delivery Rev.* **2020**, *159*, 332.
[3] S. Kamerkar, V. S. LeBleu, H. Sugimoto, S. Yang, C. F. Ruivo, S. A. Melo, J. J. Lee, R. Kalluri, *Nature* **2017**, *546*, 498.
[4] L. Alvarez-Erviti, Y. Seow, H. Yin, C. Betts, S. Lakhal, M. J. Wood, *Nat. Biotechnol.* **2011**, *29*, 341.
[5] S. Duarte-Sanmiguel, N. Higuita-Castro, D. Gallego-Perez, in *Electroporation Protocols* (S. Li, L. Chang, J. Teissie), Humana, New York, NY **2020**, pp. 79–84.
[6] L. R. Lemmerman, M. H. H. Balch, J. T. Moore, D. Alzate-Correa, M. A. Rincon-Benavides, A. Salazar-Puerta, S. Gnyawali, H. N. Harris, W. Lawrence, L. Ortega-Pineda, L. Wilch, I. B. Risser, A. J. Maxwell, S. Duarte-Sanmiguel, D. Dodd, G. P. Guio-Vega, D. M. McTigue, W. D. Arnold, S. M. Nimjee, C. K. Sen, S. Khanna, C. Rink, N. Higuita-Castro, D. Gallego-Perez, *Sci. Adv.* **2021**, *7*, eabd4735.
[7] S. Tang, A. Salazar-Puerta, J. Richards, S. Khan, J. Hoyland, D. Gallego-Perez, B. Walter, N. Higuita-Castro, D. Purmessur, *Eur. Cells Mater.* **2021**, *41*, 90.
[8] D. Gallego-Perez, D. Pal, S. Ghatak, V. Malkoc, N. Higuita-Castro, S. Gnyawali, L. Chang, W.-C. Liao, J. Shi, M. Sinha, K. Singh, E. Steen, A. Sunyecz, R. Stewart, J. Moore, T. Ziebro, R. G. Northcutt, M. Homsy, P. Bertani, W. Lu, S. Roy, S. Khanna, C. Rink, V. B. Sundaresan, J. J. Otero, L. J. Lee, C. K. Sen, *Nat. Nanotechnol.* **2017**, *12*, 974.
[9] S. W. Ferguson, J. Nguyen, *J. Controlled Release* **2016**, *228*, 179.
[10] G. Fuhrmann, I. K. Herrmann, M. M. Stevens, *Nano Today* **2015**, *10*, 397.
[11] R. Kalluri, V. S. LeBleu, *Science* **2020**, *367*, eaau6977.
[12] S. L. Maas, X. O. Breakefield, A. M. Weaver, *Trends Cell Biol.* **2017**, *27*, 172.
[13] M. Tkach, C. Théry, *Cell* **2016**, *164*, 1226.
[14] H. Saari, E. Lázaro-Ibáñez, T. Viitala, E. Vuorimaa-Laukkanen, P. Siljander, M. Yliperttula, *J. Controlled Release* **2015**, *220*, 727.
[15] M. Setti, D. Osti1, C. Richichi, B. Ortensi, M. D. Bene, L. Fornasari, G. Beznoussenko, A. Mironov, G. Rappa, A. Cuomo, M. Faretta, T. Bonaldi, A. Lorico, G. Pelicci, *Oncotarget* **2015**, *6*, 31413.
[16] Z. Yin, J. Fan, J. Xu, F. Wu, Y. Li, M. Zhou, T. Liao, L. Duan, S. Wang, W. Geng, Y. Jin, *Front. Immunol.* **2020**, *11*, 5.
[17] J. Wahlgren, T. D. L. Karlson, M. Brisslert, F. V. Sani, E. Telemo, P. Sunnerhagen, H. Valadi, *Nucleic Acids Res.* **2012**, *40*, 130.
[18] S. Duarte-Sanmiguel, V. Shukla, B. Benner, J. Moore, L. Lemmerman, W. Lawrence, A. Panic, S. Wang, N. Idzkowski, G. Guio-Vega, *Sci. Rep.* **2020**, *10*, 1189.
[19] V. C. Shukla, S. Duarte-Sanmiguel, A. Panic, A. Senthilvelan, J. Moore, C. Bobba, B. Benner, W. E. Carson III, S. N. Ghadiali, D. Gallego-Perez, *Adv. Biosyst.* **2020**, *4*, 2000049.
[20] R. Wesolowski, J. Markowitz, W. E. Carson 3rd, *J. Immunother. Cancer* **2013**, *1*, 10.
[21] A. Stiff, P. Trikha, R. Wesolowski, K. Kendra, V. Hsu, S. Uppati, E. L. McMichael, M. Duggan, A. Campbell, K. Keller, I. Landi, Y. Zhong, J. Dubovsky, J. H. Howard, L. Yu, B. Harrington, M. Old, S. Reiff, T. Mace, S. Tridandapani, N. Muthusamy, M. Caligiuri, J. C. Byrd, W. E. Carson, *Cancer Res.* **2016**, *76*, 2125.
[22] A. Stiff, P. Trikha, B. Mundy-Bosse, E. McMichael, A. Campbell, S. Gautam, D. Abood, I. Landi, V. Hsu, M. Duggan, R. Wesolowski, M. Old, J. Howard, L. Yu, N. Stasik, K. Kendra, T. Olencki, N. Muthusamy, S. Tridandipani, J. Byrd, M. Caligiuri, W. Carson, *Clin. Cancer Res.* **2018**, *24*, 1891.
[23] J. A. Dubovsky, K. A. Beckwith, G. Natarajan, J. A. Woyach, S. Jaglowski, Y. Zhong, J. D. Hessler, T. M. Liu, B. Y. Chang, K. M. Larkin, M. R. Stefanovski, D. L. Chappell, F. W. Frissora, L. L. Smith, K. A. Smucker, J. M. Flynn, J. A. Jones, L. A. Andritsos, K. Maddocks, A. M. Lehman, R. Furman, J. Sharman, A. Mishra, M. A. Caligiuri, A. R. Satoskar, J. J. Buggy, N. Muthusamy, A. J. Johnson, J. C. Byrd, *Blood* **2013**, *122*, 2539.

[24] B. L. Mundy-Bosse, G. B. Lesinski, A. C. Jaime-Ramirez, K. Benninger, M. Khan, P. Kuppusamy, K. Guenterberg, S. V. Kondadasula, A. R. Chaudhury, K. M. La Perle, M. Kreiner, G. Young, D. C. Guttridge, W. E. Carson, 3rd, *Cancer Res.* **2011**, *71*, 5101.
[25] W. He, P. Liang, G. Guo, Z. Huang, Y. Niu, L. Dong, C. Wang, J. Zhang, *Sci. Rep.* **2016**, *6*, 24506.
[26] H.-L. Huang, Y.-M. Liu, T.-Y. Sung, T.-C. Huang, Y.-W. Cheng, J.-P. Liou, S.-L. Pan, *Theranostics* **2019**, *9*, 6676.
[27] A. Celebiler, Y. Kilic, S. Saydam, T. Canda, Z. Başkan, A. I. Sevinc, M. Sakizli, *Cancer Sci.* **2009**, *100*, 2341.
[28] M. Anania, M. Sensi, E. Radaelli, C. Miranda, M. Vizioli, S. Pagliardini, E. Favini, L. Cleris, R. Supino, F. Formelli, *Oncogene* **2011**, *30*, 3011.
[29] R. K. Pachynski, P. Wang, N. Salazar, Y. Zheng, L. Nease, J. Rosalez, W.-I. Leong, G. Virdi, K. Rennier, W. J. Shin, *Front. Immunol.* **2019**, *10*, 983.
[30] Y. Liu-Chittenden, M. Jain, K. Gaskins, S. Wang, M. J. Merino, S. Kotian, S. K. Gara, S. Davis, L. Zhang, E. Kebebew, *Oncogene* **2017**, *36*, 3541.
[31] A. Stiff, P. Trikha, R. Wesolowski, K. Kendra, V. Hsu, S. Uppati, E. McMichael, M. Duggan, A. Campbell, K. Keller, *Cancer Res.* **2016**, *76*, 2125.
[32] P. Trikha, R. L. Plews, A. Stiff, S. Gautam, V. Hsu, D. Abood, R. Wesolowski, I. Landi, X. Mo, J. Phay, *Oncoimmunology* **2016**, *5*, 1214787.
[33] D. Gallego-Perez, D. Pal, S. Ghatak, V. Malkoc, N. Higuita-Castro, S. Gnyawali, L. Chang, W.-C. Liao, J. Shi, M. Sinha, *Nat. Nanotechnol.* **2017**, *12*, 974.
[34] J. Markowitz, R. Wesolowski, T. Papenfuss, T. R. Brooks, W. E. Carson, *Breast Cancer Res. Treat.* **2013**, *140*, 13.
[35] D. W. Beury, K. H. Parker, M. Nyandjo, P. Sinha, K. A. Carter, S. Ostrand-Rosenberg, *J. Leukocyte Biol.* **2014**, *96*, 1109.
[36] S. Nam, A. Lee, J. Lim, J.-S. Lim, *Biomol. Ther.* **2019**, *27*, 63.
[37] N. Higuita-Castro, D. Gallego-Perez, K. Love, M. R. Sands, G. Kaletunç, D. J. Hansford, *Ind. Biotechnol.* **2012**, *8*, 365.
[38] Y. Wu, M. C. Terp, K. J. Kwak, D. Gallego-Perez, S. P. Nana-Sinkam, L. J. Lee, *Small* **2013**, *9*, 2358.
[39] X. Zhao, X. Huang, X. Wang, Y. Wu, A. K. Eisfeld, S. Schwind, D. Gallego-Perez, P. E. Boukany, G. I. Marcucci, L. J. Lee, *Adv. Sci.* **2015**, *2*, 1500111.
[40] D. Gallego-Perez, N. Higuita-Castro, L. Denning, J. DeJesus, K. Dahl, A. Sarkar, D. J. Hansford, *Lab Chip* **2012**, *12*, 4424.
[41] D. Gallego-Perez, L. Chang, J. Shi, J. Ma, S.-H. Kim, X. Zhao, V. Malkoc, X. Wang, M. Minata, K. J. Kwak, *Nano Lett.* **2016**, *16*, 5326.
[42] S.-Q. Gu, D. Gallego-Perez, S. P. McClory, J. Shi, J. Han, L. J. Lee, D. R. Schoenberg, *Nucleic Acids Res.* **2016**, *44*, 5811.
[43] V. C. Shukla, T.-r. Kuang, A. Senthilvelan, N. Higuita-Castro, S. Duarte-Sanmiguel, S. N. Ghadiali, D. Gallego-Perez, *Trends Biotechnol.* **2018**, *36*, 549.
[44] S. P. Kerkar, R. S. Goldszmid, P. Muranski, D. Chinnasamy, Z. Yu, R. N. Reger, A. J. Leonardi, R. A. Morgan, E. Wang, F. M. Marincola, G. Trinchieri, S. A. Rosenberg, N. P. Restifo, *J. Clin. Invest.* **2011**, *121*, 4746.
[45] C. W. Shields, M. A. Evans, L. L.-W. Wang, N. Baugh, S. Iyer, D. Wu, Z. Zhao, A. Pusuluri, A. Ukidve, D. C. Pan, *Sci. Adv.* **2020**, *6*, eaaz6579.
[46] S. Kaczanowska, D. W. Beury, V. Gopalan, A. K. Tycko, H. Qin, M. E. Clements, J. Drake, C. Nwanze, M. Murgai, Z. Rae, *Cell* **2021**, *184*, 2033.
[47] W. A. Banks, P. Sharma, K. M. Bullock, K. M. Hansen, N. Ludwig, T. L. Whiteside, *Int. J. Mol. Sci.* **2020**, *21*, 4407.
[48] J. Matsumoto, T. Stewart, L. Sheng, N. Li, K. Bullock, N. Song, M. Shi, W. A. Banks, J. Zhang, *Acta Neuropathol. Commun.* **2017**, *5*, 71.
[49] X. Zhang, Y. Liu, L. Dai, G. Shi, J. Deng, Q. Luo, Q. Xie, L. Cheng, C. Li, Y. Lin, *Oncogene* **2021**, *40*, 1516.
[50] M. Mirghorbani, S. Van Gool, N. Rezaei, *Expert Rev. Neurother.* **2013**, *13*, 1395.
[51] G. Pawelec, C. P. Verschoor, S. Ostrand-Rosenberg, *Front. Immunol.* **2019**, *10*, 1099.
[52] A. Salminen, K. Kaarniranta, A. Kauppinen, *Cell. Mol. Life Sci.* **2018**, *75*, 3099.
[53] S. Sendo, J. Saegusa, A. Morinobu, *Inflammation Regener.* **2018**, *38*, 19.
[54] T. Kawano, M. Shimamura, H. Nakagami, H. Kanki, T. Sasaki, H. Mochizuki, *PLoS One* **2019**, *14*, 0215482.
[55] A. De Leo, A. Ugolini, F. Veglia, *Cells* **2020**, *10*, 18.
[56] R. Wesolowski, M. C. Duggan, A. Stiff, J. Markowitz, P. Trikha, K. M. Levine, L. Schoenfield, M. Abdel-Rasoul, R. Layman, B. Ramaswamy, *Cancer Immunol., Immunother.* **2017**, *66*, 1437.
[57] Y. S. Khaled, B. J. Ammori, *J. Immunol. Res.* **2014**, *2014*, Article ID 879897.
[58] P. Ma, P. L. Beatty, J. McKolanis, R. Brand, R. E. Schoen, O. J. Finn, *Front. Immunol.* **2019**, *10*, 1401.
[59] B. Benner, L. Scarberry, L. P. Suarez-Kelly, M. C. Duggan, A. R. Campbell, E. Smith, G. Lapurga, K. Jiang, J. P. Butchar, S. Tridandapani, *J. Immunother. Cancer* **2019**, *7*, 140.
[60] Y. Liu-Chittenden, D. Patel, K. Gaskins, T. J. Giordano, G. Assie, J. Bertherat, E. Kebebew, *J. Clin. Endocrinol. Metab.* **2016**, *101*, 3345.
[61] Y. Liu-Chittenden, M. Jain, K. Gaskins, S. Wang, M. J. Merino, S. Kotian, S. K. Gara, S. Davis, L. Zhang, E. Kebebew, *Oncogene* **2017**, *36*, 3541.
[62] B. Anand-Apte, L. Bao, R. Smith, B. Zetter, K. Iwata, B. R. Olsen, S. S. Apte, *Biochem. Cell Biol.* **1996**, *74*, 853.
[63] J. H. Qi, Q. Ebrahem, N. Moore, G. Murphy, L. Claesson-Welsh, M. Bond, A. Baker, B. Anand-Apte, *Nat. Med.* **2003**, *9*, 407.
[64] Y. J. Cha, J. S. Koo, *Cells* **2020**, *9*, 1785.
[65] J. Shi, Y. Ma, J. Zhu, Y. Chen, Y. Sun, Y. Yao, Z. Yang, J. Xie, *Molecules* **2018**, *23*, 3044.
[66] Y. Zhang, Z. Yan, X. Xia, Y. Lin, *Micromachines* **2020**, *11*, 767.
[67] C.-X. Zheng, S.-M. Wang, Y.-H. Bai, T.-T. Luo, J.-Q. Wang, C.-Q. Dai, B.-L. Guo, S.-C. Luo, D.-H. Wang, Y.-L. Yang, Y.-Y. Wang, *Anatom. Rev.* **2017**, *301*, 825.
[68] N. Nayerossadat, T. Maedeh, P. A. Ali, *Adv. Biomed. Res.* **2012**, *1*, 27.
[69] L. Chang, M. Howdyshell, W. C. Liao, C. L. Chiang, D. Gallego-Perez, Z. Yang, W. Lu, J. C. Byrd, N. Muthusamy, L. J. Lee, *Small* **2015**, *11*, 1818.
[70] L. Chang, D. Gallego-Perez, X. Zhao, P. Bertani, Z. Yang, C.-L. Chiang, V. Malkoc, J. Shi, C. K. Sen, L. Odonnell, *Lab Chip* **2015**, *15*, 3147.
[71] L. Chang, P. Bertani, D. Gallego-Perez, Z. Yang, F. Chen, C. Chiang, V. Malkoc, T. Kuang, K. Gao, L. J. Lee, *Nanoscale* **2016**, *8*, 243.
[72] L. Chang, L. Li, J. Shi, Y. Sheng, W. Lu, D. Gallego-Perez, L. J. Lee, *Lab Chip* **2016**, *16*, 4047.
[73] P. Bertani, W. Lu, L. Chang, D. Gallego-Perez, L. James Lee, C. Chiang, N. Muthusamy, *J. Vac. Sci. Technol., B: Nanotechnol. Microelectron.: Mater., Process., Meas., Phenom.* **2015**, *33*, 06F903.